



HAL
open science

Electron–Phonon Coupling in Luminescent Europium-Doped Hydride Perovskites Studied by Luminescence Spectroscopy, Inelastic Neutron Scattering, and First-Principles Calculations

Gauthier Lefevre, Alexander Herfurth, Adlane Sayede, Thomas Wylezich, Sacha Welinski, Jean-François Blach, Pedro Duarte Vaz, Stewart Parker, Philippe Goldner, Nathalie Kunkel

► **To cite this version:**

Gauthier Lefevre, Alexander Herfurth, Adlane Sayede, Thomas Wylezich, Sacha Welinski, et al.. Electron–Phonon Coupling in Luminescent Europium-Doped Hydride Perovskites Studied by Luminescence Spectroscopy, Inelastic Neutron Scattering, and First-Principles Calculations. *Journal of Physical Chemistry C*, 2018, 122 (19), pp.10501 - 10509. 10.1021/acs.jpcc.8b01011 . hal-01808502

HAL Id: hal-01808502

<https://hal.science/hal-01808502>

Submitted on 23 Nov 2023

HAL is a multi-disciplinary open access archive for the deposit and dissemination of scientific research documents, whether they are published or not. The documents may come from teaching and research institutions in France or abroad, or from public or private research centers.

L'archive ouverte pluridisciplinaire **HAL**, est destinée au dépôt et à la diffusion de documents scientifiques de niveau recherche, publiés ou non, émanant des établissements d'enseignement et de recherche français ou étrangers, des laboratoires publics ou privés.

Electron–Phonon Coupling in Luminescent Europium-Doped Hydride Perovskites Studied by Luminescence Spectroscopy, Inelastic Neutron Scattering, and First-Principles Calculations

Gauthier Lefevre,[†] Alexander Herfurth,[‡] Holger Kohlmann,[‡] Adlane Sayede,[†] Thomas Wylezich,[§] Sacha Welinski,^{||} Pedro Duarte Vaz,^{⊥,#} Stewart F. Parker,[⊥] Jean François Blach,[†] Philippe Goldner,^{||} and Nathalie Kunkel^{*,§,||}

[†]UCCS-UMR CNRS 8181, Université d'Artois, Faculté de Sciences Jean Perrin, Rue Jean Souvraz, 62300 Lens, France

[‡]Inorganic Chemistry, University of Leipzig, Johannisallee 29, 04103 Leipzig, Germany

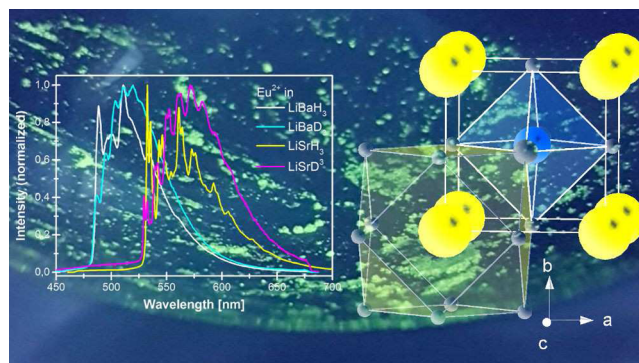
[§]Chair for Inorganic Chemistry with Focus on Novel Materials, Department Chemistry, Technical University of Munich, Lichtenbergstr. 4, 85748 Garching, Germany

^{||}Université PSL, Chimie Paris Tech, CNRS, Institut de Recherche de Chimie Paris, 11 rue Pierre et Marie Curie, 75005 Paris, France

[⊥]ISIS Facility, STFC Rutherford Appleton Laboratory, Chilton, Didcot OX11 0QX, U.K.

[#]CICECO Aveiro Institute of Materials, Departamento de Química, Universidade de Aveiro, 3810-193 Aveiro, Portugal

ABSTRACT: We present a case study on the vibrational coupling of lattice phonons to the electronic $4f^7 (^8S_{7/2})-4f^65d^1 (e_g)$ transition of divalent europium in the hydrides and deuterides LiMH_3 and LiMD_3 ($M = \text{Sr}$ and Ba). For low doping concentrations, these compounds show extraordinarily well-resolved vibronic fine structures at low temperatures. Besides luminescence emission spectroscopy of the europium-doped compounds, we carried out inelastic neutron scattering (INS) experiments of the europium-free compounds. The phonons coupling to the electronic transition are identified, and a good agreement between the vibronic and the INS data is found. The frequencies of the low-energy acoustic modes do not significantly change upon replacing hydride by deuteride, whereas a decrease by a factor of approximately $\sqrt{2}$ can be observed for the higher energy optic modes. Furthermore, we compare these experimental results to density functional calculations performed with the Vienna Ab initio Simulation Package. Knowledge of the phonons of a host material is of great importance because phonons have a large influence on the optical properties, such as line widths or luminescence quenching. Hydride-containing host lattices are an ideal model system because ^1H can easily be replaced by ^2D so that isotope effects can be investigated.



■ INTRODUCTION

Rare earth-doped compounds play an important role in many optical applications, such as phosphors and plasma screens,^{1–4} optical fibers and waveguides,⁵ bioimaging and sensors,^{6–9} or quantum information technology and spectral filtering.^{10–12} Whereas the $4f$ electrons are so well-shielded by the filled $5s^2$ and $5p^6$ shells that the crystalline environment can be considered as a weak perturbation of the free-ion level,^{10,13} the $5d$ electrons of the excited state of $4f-5d$ transitions of ions such as Eu^{2+} , Ce^{3+} , or Yb^{2+} remain unshielded and can therefore show a large energy dependence of the $5d$ barycenter and the crystal field splitting on the crystalline environment.¹⁴ As a result, very different excitation and emission energies are found, for example, for Eu^{2+} or Ce^{3+} , in different host lattices.^{15,16} Additionally, except for rare cases of very high lying $5d$ levels

and emission from, for example, the $^6P_{7/2}$ ^{17,18} or the $^6I_{7/2}$ ¹⁷ state of Eu^{2+} , the absorption and emission bands in these compounds are rather broad. For such broad $5d-4f$ emission spectra, it is, even at low temperatures, rare that a well-resolved vibrational fine structure showing coupling to several modes can be observed because the coupling strength is usually intermediate; that is, the Huang–Rhys parameter S has the value $1 < S < 5$.¹⁹ However, some rare examples exist for Ce^{3+} , Pr^{3+} , and Tb^{3+} with well-resolved spectra that show a coupling to two vibrations in double perovskites.^{20–22} Recently, new types of host materials, ionic hydrides,^{23–27} complex

hydrides,^{28,29} and mixed anionic compounds containing hydrides,^{30–33} have been studied as hosts for Eu^{2+} luminescence. Here, it was found that replacing less polarizable anions by the polarizable hydride anion can lead to wide shifts of the barycenter of the 5d levels to lower energies. However, besides the interesting properties with regard to the centroid shift and crystal field splitting, hydrides as host lattices can also serve as model systems to study the correlation of the optical properties with lattice phonons. Already in 1980, Judd predicted that vibronic intensities increase with the degree of covalency,^{19,34} which is directly connected to the anion polarizability. Thus, ideal candidates for such studies are compounds with polarizable anions, such as nitrides or hydrides. Moreover, the replacement of ^1H by ^2D is an elegant tool for such studies. Knowledge on the relation between lattice phonons and electronic transitions is of great importance because phonons can have a large influence on the optical properties, such as line widths, luminescence quenching, or the efficiency of upconversion processes.^{35–39}

Here, we present a case study of LiMH_3 and LiMD_3 ($M = \text{Sr}$ and Ba), which crystallize in the inverse cubic perovskite structure type in the space group $Pm\bar{3}m$ (see Figure 1).^{24,40–42} LiEuH_3 shows the same structure⁴³ with similar lattice parameters as those observed in LiSrH_3 , and we assume that Eu^{2+} will occupy the M^{2+} site in doped compounds.

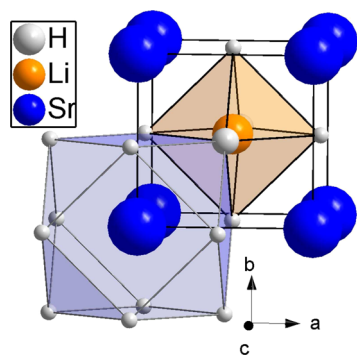


Figure 1. Crystal structure of LiSrH_3 showing the cuboctahedral surrounding of strontium and the octahedral coordination of lithium.

The Eu^{2+} -doped compounds represent an ideal model system for investigations of the vibrational coupling. In our previous study,²⁴ where we reported on the luminescence properties of samples with rather high europium concentrations, we were already able to detect some vibrational fine structure at low temperatures. Here, we use highly diluted samples (europium concentrations of approx. 0.005%) in order to obtain a better resolution of the fine structure. We carried out photoluminescence (PL) measurements on the samples with low europium concentrations as well as inelastic neutron scattering (INS) of the europium-free compounds LiBaH_3 , LiBaD_3 , and LiSrH_3 at 20 K. In an earlier work, we had confirmed the absence of phase transitions down to 10 K.²⁴ The obtained results are compared with the phonon dispersion curves and densities of states obtained by first-principles calculations.

METHODS

Synthesis. Eu^{2+} -doped samples LiMH_3 and LiMD_3 ($M = \text{Sr}$ and Ba) for PL measurements were prepared by hydrogenation of the alloys. Alloys were synthesized by melting reactions of the elements (strontium, Alfa Aesar, distilled dendritic pieces

99.8%; europium rod, Alfa Aesar 99.8%; barium rod, Chempur, 99.3% (rest strontium); and lithium, Alfa Aesar 99.8%; all were mechanically surface-cleaned) in niobium ampoules (at approx. 1100 K, depending on the metals used). In order to obtain low europium concentrations, samples of Sr:Eu with 0.5 mol % were prepared first and then diluted in order to reach the desired concentrations. Then, the alloys were hydrogenated in a hydrogen resistant autoclave (Inconel 718) at approx. 750 K and 100 bar H_2 -pressure for 2–3 days (H_2 Praxair 99.8%, D_2 Praxair 99.8%). These samples contained no or only small amounts of the binary hydrides. Large amounts of europium-free LiMH_3 and LiMD_3 ($M = \text{Sr}$ and Ba) samples for INS experiments were prepared from the binary hydrides (MH_2 had been obtained by hydrogenation of the metal before; starting materials: LiH , abcr, 99.0%; LiD , abcr, 99.4%; barium, Chempur, 99.3%; and strontium, Chempur, 99.0%). The binary hydrides were mixed and heated in a hydrogen resistant autoclave (Inconel 718) at approx. 850 K and 20–40 bar for 2–5 days. Some of these samples contained more than 25% of the binary hydrides (compositions of the samples are given in the Supporting Information, Table S2). As large amounts of samples are needed for INS, the first synthesis approach was not suitable here, and the presence of unreacted binary hydrides could not be avoided completely. Because of moisture sensitivity, all starting materials and products were handled in an argon-filled glovebox.

X-ray Diffraction. Laboratory powder X-ray diffraction (PXRD) data of the samples used for INS were collected on a Huber G670 diffractometer with Guinier geometry at $T = 297(2)$ K with $\text{Cu K}\alpha_1$ radiation. Laboratory PXRD data of the samples used for PL measurements were collected on a STOE Stadi P powder diffractometer (Stoe & Cie GmbH) with $\text{Cu K}\alpha_1$ radiation (Ge(111) monochromator) and a Dectris Mythen DCS 1K detector. For both cases, flat transmission samples with Apiezon grease between two Kapton foils were used. Crystal structures were refined using the program TOPAS (TOPAS version 5; Bruker AXS, www.bruker-axs.com). Refined lattice parameters and the amount of residual binary hydride (deuteride) are given in the Supporting Information (Table S2).

PL Measurements. PL spectra were recorded on a setup constructed in-house with a tunable optical parametric oscillator pumped by an Nd:YAG laser (Ekspla NT342B-SH with 6 ns pulse length) as the excitation source, a Jobin-Yvon HR250 monochromator, and a PI-Max ICCD camera for detection. Samples (enclosed in silica tubes of about 5 mm diameter) were placed in a closed-cycle helium cryostat (Janis CTI-Cryogenics Model CCS-150, together with a LakeShore temperature controller) and attached to the sample holder using high purity silver paint and copper sheets. Decay curves were recorded using a Jobin-Yvon HR250 monochromator and a photomultiplier tube.

Inelastic Neutron Scattering. INS experiments were carried out at the high-resolution broad-band spectrometer TOSCA (an indirect geometry time-of-flight spectrometer)^{44,45} at the ISIS Facility at 20 K. The signal was collected by detector banks in forward and backward scattering, and for data analysis, the arithmetical average of those was used. To minimize the background, short-time high-energy neutrons and the Γ -flash were removed by a NIMONIC chopper. Additionally, the tail cutter of the chopper also removes low-energy neutrons in order to prevent frame overlap. The beam size of the instrument is about $4 \times 4 \text{ cm}^2$. Samples were loaded into

indium-wire-sealed, flat-plate aluminum cans in an argon-filled glovebox. Because MH_2 and MD_2 ($M = \text{Sr}$ and Ba) were present in the corresponding samples, spectra of the binary hydrides were taken from the literature^{46,47} for subtraction or comparison.

Density Functional Calculations. Density functional calculations were carried out using the Vienna Ab initio Simulation Package (VASP)^{48–50} Version 5.4.1 together with projector augmented wave (PAW).^{51,52} The Perdew–Burke–Ernzerhof generalized gradient approximation (GGA)⁵³ was used to evaluate the exchange and correlation energies. PAW potentials with the valence electrons $5s^25p^66s^2$ for Ba and $4s^24p^65s^2$ for Sr atoms were used. In order to guarantee the reliability of the results, an optimization of the cutoff energies as well as the k -point meshes was carried out. For lithium strontium and lithium barium hydride, convergence for the total energy was obtained with a $9 \times 9 \times 9$ Monkhorst–Pack grid centered at the Γ -point, resulting in 35 k -points in the first irreducible Brillouin zone and a plane-wave expansion cutoff of 1000.0 eV. Lattice parameters and atomic positions were optimized by the minimization of the Hellmann–Feynman forces using a quasi-Newton algorithm. Criteria of 10^{-6} eV per Å and 10^{-9} eV were adopted for the convergence of the total energy and Hellmann–Feynman forces, respectively. All performed calculations were non-spin-polarized because the compounds are known to be nonmagnetic. Phonon dispersion curves were calculated with the PHONOPY code⁵⁴ using the density functional perturbation theory.

RESULTS

Vibronic Transitions. Theoretical Considerations. Electron–phonon interactions can give rise to vibronic transitions, which are optical transitions that simultaneously show a change in the electronic state and the vibrational state of the system.¹⁹ For weak electron–phonon interactions, rather sharp lines can be observed,¹⁰ whereas a strong electron–phonon interaction yields broad bands and the influence of phonons also shows a temperature dependence.³⁵

For a transition between two electronic states $\Psi_{(\text{electronic ground state}, n)}$ and $\Psi_{(\text{electronic excited state}, n')}$ with different initial and final vibrational states, the matrix element is given as follows:

$$\langle \Psi_{(\text{electronic ground state}, n)} | \vec{\mu} | \Psi_{(\text{electronic excited state}, n')} \rangle \quad (1)$$

with the transition electric dipole operator $\vec{\mu}$.¹⁹ The optical transition can consist of a number of vibronic transitions for the vibrational states $n' - n$. However, in the present study, we consider the case of low temperature, where we assume that only the lowest vibrational level of the initial electronic state will be occupied. As a consequence, we only need to consider transitions between the vibrational states $0 - n$. The $0 - 0$ transition is the zero phonon line, ZPL.

A symmetry analysis for the inverse cubic perovskite structure of LiMH_3 ($M = \text{Sr}, \text{Ba}$) in the space group type $Pm\bar{3}m$ (corresponding to the point group O_h in Schönflies notation) yields one acoustic mode of the irreducible representation T_{1u} and four optical modes,^{55–58} which are all triply degenerate. Three of the optical modes belong to the IR-active representation T_{1u} , whereas one mode is hyper-Raman-active and belongs to the representation T_{2u} . The representations Γ of the acoustic and optical modes are given by

$$\Gamma_{\text{acoustic}} = T_{1u} \quad (2)$$

$$\Gamma_{\text{optic}} = T_{2u} + 3T_{1u} \quad (3)$$

Because we can expect Eu^{2+} to occupy the strontium or barium site 1b, its surrounding consists of a cuboctahedron and consequently the lowest lying $5d^1$ level will be the two-fold-degenerate 2E_g state. To determine if an optical transition is electric-dipole-allowed, the matrix element from eq 1 can be evaluated as a product of irreducible representations with $\vec{\mu}$ transforming as T_{1u} .^{19,59} Because in our case, the $\text{Eu}^{2+} 4f^7 - 5d^1$ transition is parity allowed, we can assume that this product contains A_{1g} :

$$[\Gamma_{\text{electronic ground state}} \times T_{1u} \times \Gamma_{\text{electronic excited state}}] \supset A_{1g} \quad (4)$$

The matrix element of a vibronic transition that couples with phonons belonging to the representation T_{1u} corresponds to the product

$$[\Gamma_{\text{electronic ground state}} \times T_{1u} \times T_{1u} \times \Gamma_{\text{electronic excited state}} \times T_{1u}] \quad (5)$$

and because

$$[T_{1u} \times T_{1u}] \supset A_{1g} \quad (6)$$

we conclude that the product in eq 5 contains A_{1g} and therefore the vibronic transition is allowed.

If we repeat this procedure for the hyper-Raman mode that belongs to the representation T_{2u} , we find that a transition involving a coupling of the electronic transition and the hyper-Raman mode belonging to T_{2u} is forbidden. In the PL spectra of the Eu^{2+} -doped perovskites showing the electric dipole $4f^7 ({}^8S_{7/2}) - 4f^65d^1 (e_g)$ transition, we therefore expect to only observe a coupling of the electronic transition with the IR-active modes of the representation T_{1u} .

PL Emission Spectra. As already reported in previous results,²⁴ for $M = \text{Sr}$, the inverse perovskites $\text{LiMH}_3:\text{Eu}^{2+}$ and $\text{LiMD}_3:\text{Eu}^{2+}$ show an intense broad band emission in the yellow region, whereas the barium compounds emit in the green region. Below approximately 80 K, a vibrational fine structure starts to appear, which becomes very well-resolved at low temperatures. Decay times were in the range of those reported in the literature²⁴ or slightly longer, which is probably due to the low europium concentrations. In Figure 2, the emission spectra at 20 K under laser excitation at 350 nm are shown.

Doped with only 0.005% Eu^{2+} , all compounds show more resolved vibrational fine structures than those observed in previous results with higher doping levels,²⁴ and the resolution

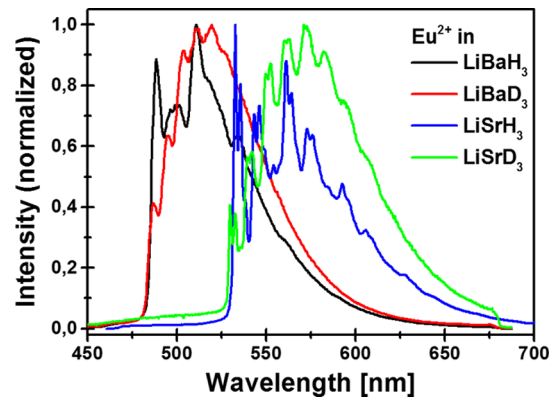


Figure 2. PL emission spectra of Eu^{2+} (0.005%) in LiMH_3 and LiMD_3 ($M = \text{Sr}$ and Ba) at 20 K. $\lambda_{\text{ex}} = 350$ nm.

is especially good for $M = \text{Sr}$. As observed before, the vibronic fine structures are more pronounced for the hydrides than for the deuterides. To determine the phonon energies, the energy of the ZPL was subtracted from the spectra. The energies of the vibronic lines are listed in Table 1, and a pictorial assignment is shown for $\text{LiSrH}_3:\text{Eu}^{2+}$ in Figure 3.

Table 1. Vibronic Transitions in the PL Emission Spectra at 20 K for the Eu^{2+} Transition $4f^65d^1-4f^7(^8S_{7/2})$ in LiMH_3 and LiMD_3 ($M = \text{Sr}$ and Ba) (Eu^{2+} 0.005%)^a

| line | LiSrH_3 [cm^{-1}] | LiSrD_3 [cm^{-1}] | LiBaH_3 [cm^{-1}] | LiBaD_3 [cm^{-1}] |
|---------------|---------------------------------------|---------------------------------------|---------------------------------------|---------------------------------------|
| ν_{1-0-0} | 105 | 105 | 92 | 92 |
| ν_{2-0-0} | 200 | 200 | 183 | 183 |
| ν_{0-1-0} | 367 | 258 | 340 | 270 |
| ν_{1-1-0} | 468 | 351 | 430 | 366 |
| ν_{2-1-0} | 568 | 440 | 530 | 450 |
| ν_{0-2-0} | 735 | 518 | 715 | 560 |
| ν_{1-2-0} | 835 | 618 | | |
| ν_{0-0-1} | 956 | 690 | 890 | 630 |
| ν_{1-0-1} | 1060 | 788 | 990 | 719 |
| ν_{2-0-1} | 1170 | 894 | 1080 | 815 |
| ν_{0-1-1} | 1320 | 950 | 1226 | |
| ν_{1-1-1} | 1418 | 1040 | | |
| ν_{2-1-1} | 1515 | 1127 | | |
| ν_{0-2-1} | 1683 | 1200 | | |
| ν_{0-0-2} | 1902 | 1380 | | |
| ν_{1-0-2} | 2000 | | | |

^aEnergies are given with respect to their ZPLs. Assignments in LiSrH_3 were made based on very well-resolved spectra, whereas the spectra for $M = \text{Ba}$ are less well-resolved so that larger errors in the correct assignment may be expected.

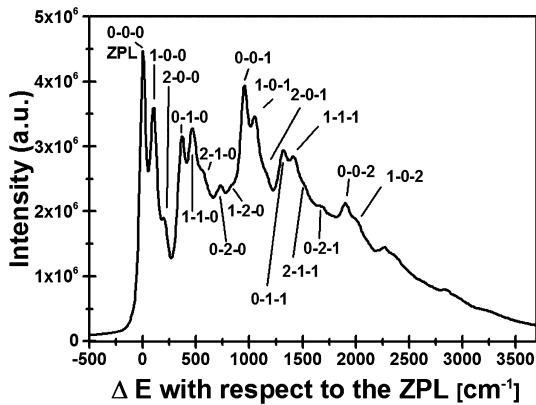


Figure 3. PL emission spectrum of Eu^{2+} (0.005%) in LiSrH_3 at 20 K. $\lambda_{\text{ex}} = 350$ nm. Energies ΔE are given with respect to the ZPL.

The well-resolved vibronic pattern shows a coupling with at least three vibrations. For $\text{LiSrH}_3:\text{Eu}^{2+}$, three lines separated by about 100 cm^{-1} are repeated at about 370 cm^{-1} . The 100 cm^{-1} line is not affected by replacing hydride by deuteride. Upon substitution of hydrogen by deuterium, we expect vibration frequencies to decrease by the square root of the reduced mass ratio, for example, approximately square root of two, if hydrogen or deuterium atoms are strongly involved in these modes. We therefore conclude that mainly the metal atoms contribute to the mode. At approximately 960 cm^{-1} , another strong line is observed, which shows replicas separated by approximately 100 cm^{-1} . Additionally, overtones involving further combinations of the modes are found. We have labeled

the lines using the notation ν_{x-y-z} where x , y , and z stand for the number of vibrations involved in the 100 cm^{-1} (x), 370 cm^{-1} (y), and 960 cm^{-1} modes, respectively. On the basis of our considerations regarding the allowed coupling of modes to the electronic transition in section **Vibronic Transitions—Theoretical Considerations**, we assume that the 370 and 960 cm^{-1} modes belong to the optical T_{1u} representations. A comparison with vibrational spectra in the literature⁵⁸ suggests that one additional mode belonging to one of the optical T_{1u} representations should be found at around 1100 cm^{-1} . However, in this spectral region, several lines from different overtones coincide so that it is difficult to correctly assign the fourth allowed vibration. Thus, we limited the assignment to the vibrational couplings that we believe can be safely identified. We repeated the assignment for $\text{LiSrD}_3:\text{Eu}^{2+}$ as well as the barium compounds. In the latter, we refrained from assigning the higher overtones because the spectra are less well-resolved.

Inelastic Neutron Scattering. In contrast to the vibrational coupling in the electronic spectra, no selection rules hold for INS, and INS is also not restricted to the center of the Brillouin zone. Because of the large incoherent neutron scattering cross section of hydrogen, it is an especially powerful tool for studying hydrides. According to ref 60, the incoherent neutron scattering cross sections for ^1H , ^2D , $^{\text{nat}}\text{Li}$, $^{\text{nat}}\text{Sr}$, and $^{\text{nat}}\text{Ba}$ are $80.27(6)$, $2.05(3)$, $0.92(3)$, $0.06(11)$, and $0.15(11)$ barn, respectively. However, because the cross section for ^1H is so much larger than those of the other elements involved, vibrations involving a high degree of hydrogen motion in the spectra will lead to enhanced signals, which can act as an effective selection rule.⁶¹ Small amounts of ^1H impurities in $^2\text{D}_2$ might also have a large influence on the spectral properties. Furthermore, in INS, multiple scattering processes (overtones and combinations) involving two or more $1-0$ transitions are allowed and may also be observed.

In Figure 4, the INS spectrum of LiSrH_3 is displayed. Because the samples contained SrH_2 (as detected by PXRD;

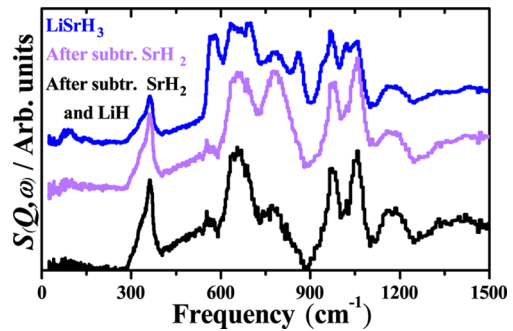


Figure 4. Frequency distributions for LiSrH_3 as measured and LiSrH_3 after subtracting the spectra of SrH_2 and LiH . Recorded at TOSCA at 20 K.

see the **Supporting Information**), the spectrum of SrH_2 was subtracted from the measured data.

The frequency distribution measured for LiSrH_3 shows vibrational modes at approximately 100 , 360 , 560 , 650 , 970 , and 1160 cm^{-1} . The modes at 100 , 360 , and 970 cm^{-1} are in very good agreement with the data obtained from the analysis of the vibrational coupling to the Eu^{2+} $4f-5d$ transition and can be assigned to the modes ν_{1-0-0} , ν_{0-1-0} , and ν_{0-0-1} , respectively, where ν_{0-1-0} and ν_{0-0-1} are optical modes belonging to the representation T_{1u} . The mode at 560 cm^{-1} can be assigned to

the replica ν_{2-1-0} . Furthermore, the mode at 1160 cm^{-1} is assigned to a further optical mode of the representation T_{1u} , which cannot be clearly identified in the PL spectrum because of overlaying replicas. Consequently, we assign the mode at 650 cm^{-1} to the optical mode of the representation T_{2u} with a hyper-Raman activity, which cannot couple to the electric dipole transition of Eu^{2+} .

We also studied LiBaH_3 and LiBaD_3 by means of INS (data are given in the [Supporting Information](#), Figure S1). For both compounds, a mode at 90 cm^{-1} is found, which is in good agreement with the optical spectra. Furthermore, the ν_{0-1-0} mode can be assigned at 340 cm^{-1} for the hydride and 300 cm^{-1} for the deuteride. For LiBaH_3 , also the ν_{0-0-1} is observed at $\sim 890\text{ cm}^{-1}$. However, the quality of the data is not as good as in the case of the strontium compound.

Density Functional Calculations. For further clarifications, we also carried out first-principles calculations using a supercell approach, as described in section [Methods—Density Functional Calculations](#). The equilibrium lattice constants determined from Birch–Murnaghan fourth-order equation of states and the corresponding mechanical properties (bulk, Shear, and Young’s moduli) are summarized in [Table 2](#). The results are in good agreement with experiments and other theoretical work.^{62,63}

Table 2. Calculated Structural and Elastic Parameters of LiBaH_3 , LiBaD_3 , LiSrH_3 , and LiSrD_3 at Zero Pressure

| | a_0 (Å) | B (GPa) ^a | G (GPa) ^b | E (GPa) ^c | ν ^d |
|------------------------------------|-----------|------------------------|------------------------|------------------------|--------------------|
| LiBaH_3 | | | | | |
| calc. this work | 4.020 | 37.59 | 39.30 | 87.43 | 0.112 |
| mBJ & GGA ⁶³ | 4.005 | 37.536 | 38.924 | | 0.115 |
| GGA ⁶² | 3.989 | 37.83 | 39.99 | 87.48 | 0.093 |
| exp. this work | 4.014 | | | | |
| LiBaD_3 | | | | | |
| calc. this work | 4.020 | 37.25 | 39.33 | 87.27 | 0.109 |
| exp. this work | 4.008 | | | | |
| LiSrH_3 | | | | | |
| calc. this work | 3.808 | 42.68 | 46.11 | 101.70 | 0.103 |
| mBJ & GGA ⁶³ | 3.81 | 42.970 | 46.019 | | 0.100 |
| GGA ⁶² | 3.788 | 34.15 | 47.14 | 103.44 | 0.096 |
| exp. this work | 3.825 | | | | |
| LiSrD_3 | | | | | |
| calc. this work | 3.808 | 42.47 | 46.12 | 101.59 | 0.101 |
| exp. this work | 3.818 | | | | |

^aBulk. ^bShear modulus. ^cYoung’s modulus. ^dPoisson’s ratio.

Figures 5 and 6 show the dispersion and the phonon density of states (phonon DOS) of LiSrH_3 and LiSrD_3 . For both the hydride and the deuteride, a low-energy acoustic branch is observed, which appears at $\sim 110\text{ cm}^{-1}$ (0 cm^{-1} at the Γ -point). This is in good agreement with the mode found in the INS data (100 cm^{-1}). At 360 cm^{-1} , another intense mode can be found in the calculated LiSrH_3 spectra and assigned to the T_{1u} optical representation. This is also in good agreement with the mode found for the vibrational coupling to the Eu^{2+} electronic transition (367 cm^{-1}) and the mode found in the INS spectra (360 cm^{-1}). In the calculated phonon DOS for the deuteride LiSrD_3 , the agreement with the vibronic coupling of this mode is not as good as in the case of the hydride; the calculated mode at around 310 cm^{-1} seems to correspond to the ν_{0-1-0} mode found at 260 cm^{-1} in the experimental data. In the calculated spectra, this corresponds to a decrease in energy of about 13%

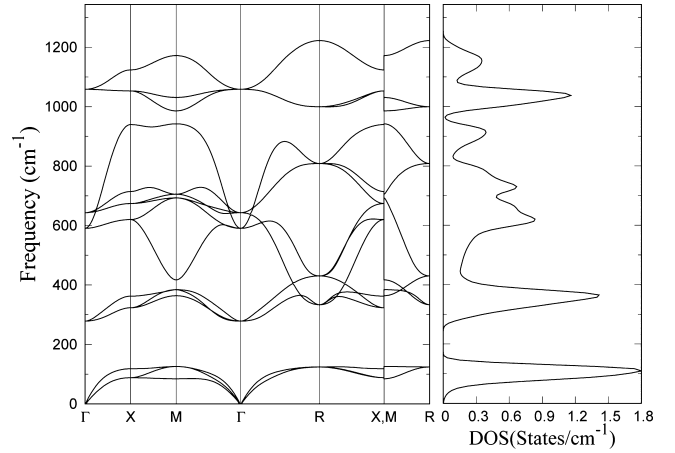


Figure 5. Phonon dispersion and DOS of LiSrH_3 as calculated by using VASP.

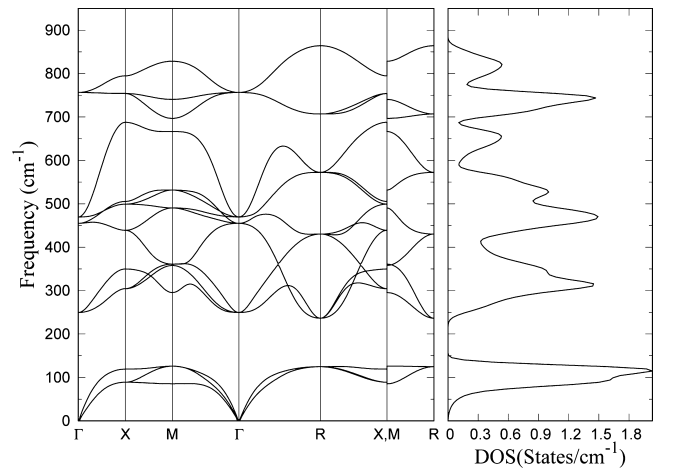


Figure 6. Phonon dispersion and DOS of LiSrD_3 as calculated by using VASP.

from hydride to deuteride. Further modes can be found at ~ 620 , ~ 730 , ~ 920 , and $\sim 1160\text{ cm}^{-1}$ in the calculated spectra of LiSrH_3 . The mode at 620 cm^{-1} likely corresponds to the mode observed at 650 cm^{-1} by INS. Modes at 920 and 1160 cm^{-1} are likely to correspond to the 970 and 1160 cm^{-1} modes, respectively, found by PL and INS measurements.

Comparison of the calculated spectra of the hydride LiSrH_3 and LiSrD_3 (Figure 7) shows an approximate ratio of $\sqrt{2}$ for the frequencies of the higher energy modes, which is expected for optical phonons.⁶⁴

The corresponding phonon distributions and phonon DOSs for the barium compounds are shown in the [Supporting Information](#) (Figures S2–S4). Furthermore, the partial phonon DOSs for LiBaH_3 (a), LiBaD_3 (b), LiSrH_3 (c), and LiSrD_3 (d) are shown in [Figure 8](#). As expected, the heavy atoms barium and strontium have their quasi-global contribution to the acoustical region, whereas the contributions of lithium and hydride are found in the optical region. For deuterides, the lithium vibrations seem to be more spread to higher optical phonon frequencies.

DISCUSSION

In order to summarize the results obtained by different methods, a comparison of the values and the assignment of the

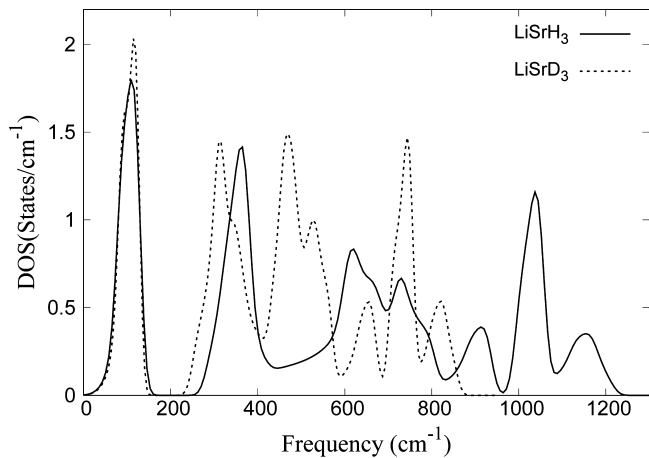


Figure 7. Comparison of the phonon DOSs of the hydride LiSrH₃ and the deuteride LiSrD₃ as calculated by using VASP.

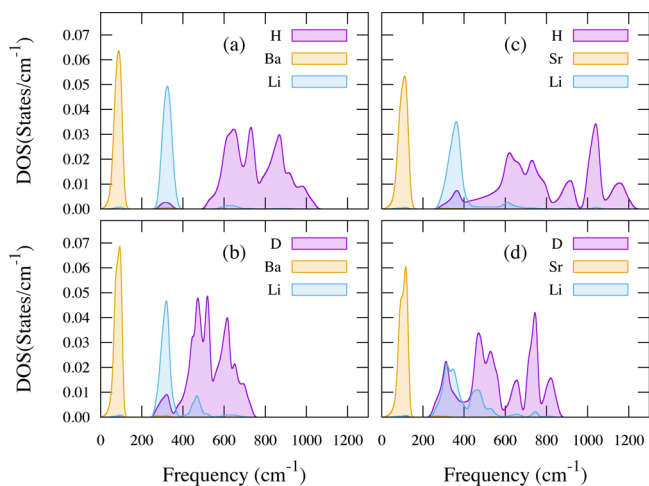


Figure 8. Comparison of the partial phonon DOSs for LiBaH₃ (a), LiBaD₃ (b), LiSrH₃ (c), and LiSrD₃ (d) as calculated by using VASP.

fundamental modes found in the PL spectra, the inelastic neutron spectra, and the density functional calculations are given in Table 3. Whereas the vibrational modes are clearly resolved in the PL spectra for the strontium compounds, the resolutions are less good for the barium compounds. Thus, the assignment of the modes for the barium compounds can be expected to be less exact.

As already mentioned in section Results—PL Emission Spectra, comparison of the vibrations in the different compounds shows that the mode ν_{1-0-0} and its replicas do not show any decrease of their frequencies by a factor of $\sqrt{2}$ upon replacing hydride by deuteride. We explain this observation by the fact that acoustic modes will be less affected by isotope effects than optical modes⁶⁴ because the isotopic shift will be proportional to the total mass of all ions in the unit cell because they all participate in the mode; thus, deuteration will have a negligible effect on the transition energy. However, there is a significant change in the intensity of the ZPL when hydrides and deuterides are compared. Moreover, the 100 cm⁻¹ mode in the PL spectra seems to correspond to an acoustic mode, even though it is unexpected to observe it in the optical spectra. The nature of these transitions remains unclear. For the higher energy modes ν_{0-1-0} , ν_{0-0-1} and their replicas, a decrease of the frequencies by a factor of $\sqrt{2}$ upon replacing

Table 3. Comparison of the Fundamental Modes Found in the PL Emission Spectra at 20 K for the Eu²⁺ Transition 4f⁶5d¹–4f⁷(⁸S_{7/2}), the Inelastic Neutron Spectra, and the Density Functional Calculations Given in cm⁻¹

| | PL | INS | DFT |
|--------------------------|-----|------|------|
| LiSrH₃ | | | |
| T_{1u} acoustic | 105 | 100 | 110 |
| T_{1u} optic | 367 | 360 | 360 |
| T_{2u} optic | | 650 | 620 |
| T_{1u} optic | 956 | 970 | 920 |
| T_{1u} optic | | 1160 | 1160 |
| LiSrD₃ | | | |
| T_{1u} acoustic | 105 | | 110 |
| T_{1u} optic | 258 | | 310 |
| T_{2u} optic | | | 460 |
| T_{1u} optic | 690 | | 660 |
| T_{1u} optic | | | 820 |
| LiBaH₃ | | | |
| T_{1u} acoustic | 92 | 90 | 90 |
| T_{1u} optic | 340 | 340 | 330 |
| T_{2u} optic | | 650 | 650 |
| T_{1u} optic | 890 | 890 | 890 |
| T_{1u} optic | | 950 | 930 |
| LiBaD₃ | | | |
| T_{1u} acoustic | 92 | 90 | 90 |
| T_{1u} optic | 270 | 300 | 330 |
| T_{2u} optic | | 450 | 440 |
| T_{1u} optic | 630 | 620 | 625 |
| T_{1u} optic | | 670 | 650 |

hydride by deuteride can be approximately observed. For example, in the optical spectra, we find about 370 cm⁻¹ for ν_{0-1-0} in LiSrH₃:Eu²⁺ and only \sim 260 cm⁻¹ in the corresponding deuterides. In the optical spectra of the barium compound, the ν_{0-1-0} mode can be found at 340 cm⁻¹ for the hydride and \sim 270 cm⁻¹ for the deuteride. For the third mode ν_{0-0-1} , \sim 960 cm⁻¹ is found in LiSrH₃:Eu²⁺ and 690 cm⁻¹ for LiSrD₃:Eu²⁺. In the barium compound, ν_{0-0-1} appears at 890 cm⁻¹ in the hydride and 630 cm⁻¹ in the deuteride. In conclusion, we assign the optical mode in LiSrH₃ at 370 cm⁻¹, which can also be observed in both INS and PL data, to a Sr–(LiH₃) stretching mode (T_{1u}) and the mode at 1160 cm⁻¹, which could only clearly be identified in the INS data, to a Li–H stretching mode (T_{1u}). Both assignments are in good agreement with the literature data for cubic perovskites.^{57,58} For the two remaining modes at 650 (only observed in the INS, not the optical spectra) and 970 cm⁻¹, which both correspond to Li–H-bending modes, we propose a different assignment. In contrast to earlier suggestions⁵⁸ and on the basis of the selection rules for the coupling of vibrational modes to the electric dipole 4f–5d transition of Eu²⁺, we suggest to assign the mode at 650 cm⁻¹ to the T_{2u} representation and the mode at 970 cm⁻¹ to T_{1u} . The assignment in the deuteride and the barium compounds can be carried out accordingly; however, the resolution of the optical spectra is not as good as for the strontium compounds, and also the quality of our INS data is lower. The low-energy modes assigned to acoustic modes do not show any decrease of their frequencies by a factor of $\sqrt{2}$ upon replacing hydride by deuteride, whereas the modes assigned to optical modes do.

Information on the vibrational modes can also be interesting for the understanding of the optical thermal stabilities of the

compounds. A comparison of the luminescence quenching temperatures for the different perovskites²⁷ obtained from luminescence emission lifetime measurements yielded luminescence quenching temperatures ($T_{50\%}$) of 165 K for LiSrH_3 , 175 K for LiSrD_3 , 210 K for LiBaH_3 , and 230 K for LiBaD_3 . From the luminescence quenching temperatures ($T_{50\%}$), it is possible to estimate the energy barrier ΔE for thermal quenching (difference between the relaxed lowest d-states and the conduction band) using the simple equation³⁷

$$\Delta E = \frac{T_{50\%}}{680} [\text{eV}] \quad (7)$$

The phonon energies are directly related to the photoionization behavior because thermal quenching in such systems follows an Arrhenius relation, where the temperature dependence of the luminescence emission intensity is given as follows:^{27,37}

$$I(T) = \frac{I(0)}{1 + \frac{\Gamma_0}{\Gamma_v} \exp\left(\frac{-\Delta E}{k_B T}\right)} \quad (8)$$

where k_B is Boltzmann's constant, ΔE is the energy barrier for thermal quenching, Γ_v is the radiative decay rate of the Eu^{2+} 5d states, and Γ_0 is the attempt rate for thermal quenching. It is well-known that the attempt rate has a magnitude similar to that of the maximum phonon frequency.³⁸ Consequently, the observed higher phonon energies in hydrides are responsible for the observed slightly faster thermal quenching in hydrides. The situation is less clear for the substitution of strontium with barium. It may be suggested that the slightly higher phonon frequencies in the strontium compounds also play a role; however, the different sizes of the band gaps or the different position of the conduction band may have a larger impact.

CONCLUSIONS

In summary, the combination of highly well-resolved vibrational fine structures in the Eu^{2+} 5d–4f luminescence emission, especially for $\text{LiSrH}_3:\text{Eu}^{2+}$, INS experiments, and density functional calculations allowed the assignment of several vibrational modes, and we observed a decrease in the energies of the optic modes upon replacing hydride by deuteride. Because substitution of hydride by deuteride leads to a doubling of the anion mass, hydrides are ideal candidates for such studies, and the results show that the combination of resolved fine structures in rare earth-doped samples showing PL and INS, as well as calculations, represent a powerful tool for the investigation of lattice phonons in ionic hydrides. It is also possible to directly relate the photoionization behavior to the changes in the vibrational frequencies which result from the substitution of hydride by deuteride. To gain a better overview, it may be worthwhile to extend the combination of studies using INS as well as the determination of optical properties, such as the luminescence quenching temperature, to other hydride- and deuteride-containing host materials as well as other materials with polarizable anions, such as nitrides, in the future.

ACKNOWLEDGMENTS

The authors would like to thank the ISIS Neutron and Muon Source for beamtime at TOSCA and Jean-François Engrand for constructing a sample holder for low-temperature PL measurements using ampoules. N.K. and T.W. would like to thank the Fonds der Chemischen Industrie for a Liebig and a doctoral fellowship (Li 197/02) and Prof. Fässler for hosting our group. A.H. and H.K. would like to thank the DFG for financial support (KO1803/7-1). P.G., N.K., S.W., and T.W. thank the Bavarian–French Academy Center for a mobility aid for their French–German collaboration (Az. FK03-2017). Furthermore, A.S., H.K., and N.K. thank the Université d'Artois for financial support for a French–German exchange.

REFERENCES

- (1) Schnick, W. Shine a Light with Nitrides. *Phys. Status Solidi RRL* **2009**, *3*, A113–A114.
- (2) Jüstel, T.; Nikol, H.; Ronda, C. New Developments in the Field of Luminescent Materials for Lighting and Displays. *Angew. Chem., Int. Ed.* **1998**, *37*, 3084–3103.
- (3) Feldmann, C.; Jüstel, T.; Ronda, C. R.; Schmidt, P. J. Inorganic Luminescent Materials: 100 Years of Research and Application. *Adv. Funct. Mater.* **2003**, *13*, 511–516.
- (4) Höpfe, H. A. Recent Developments in the Field of Inorganic Phosphors. *Angew. Chem., Int. Ed.* **2009**, *48*, 3572–3582.
- (5) Eliseeva, S. V.; Bünzli, J.-C. G. Rare Earths: Jewels for Functional Materials of the Future. *New J. Chem.* **2011**, *35*, 1165–1176.
- (6) Bünzli, J.-C. G.; Piguët, C. Taking Advantage of Luminescent Lanthanide Ions. *Chem. Soc. Rev.* **2005**, *34*, 1048–1077.
- (7) Binnemans, K. Lanthanide-Based Luminescent Hybrid Materials. *Chem. Rev.* **2009**, *109*, 4283–4374.
- (8) Bünzli, J.-C. G.; Eliseeva, S. V. Intriguing Aspects of Lanthanide Luminescence. *Chem. Sci.* **2013**, *4*, 1939–1949.
- (9) Müller-Buschbaum, K.; Beuerle, F.; Feldmann, C. MOF Based Luminescence Tuning and Chemical/Physical Sensing. *Microporous Mesoporous Mater.* **2015**, *216*, 171–199.
- (10) Thiel, C. W.; Böttger, T.; Cone, R. L. Rare-Earth-Doped Materials for Applications in Quantum Information Storage and Signal Processing. *J. Lumin.* **2011**, *131*, 353–361.
- (11) Goldner, P.; Ferrier, A.; Guillot-Noël, O. Chapter Rare Earth-Doped Crystals for Quantum Information Processing. In *Handbook on the Physics and Chemistry of Rare Earths*; Bünzli, J.-C. G., Pecharsky, V. K., Eds.; North Holland, Amsterdam, 2015; pp 1–78.
- (12) Kunkel, N.; Goldner, P. Recent Advances in Rare Earth Doped Inorganic Crystalline Materials for Quantum Information Processing. *Z. Anorg. Allg. Chem.* **2018**, *644*, 66–76.
- (13) Macfarlane, R. M. High-Resolution Laser Spectroscopy of Rare-Earth Doped Insulators: a Personal Perspective. *J. Lumin.* **2002**, *100*, 1–20.

- (14) Blasse, G.; Grabmeier, B. C. *Luminescent Materials*; Springer, Berlin, 1994.
- (15) Dorenbos, P. Energy of the First $4f^7$ - $4f^6$ 5d Transition of Eu^{2+} in Inorganic Compounds. *J. Lumin.* **2003**, *104*, 239–260.
- (16) Dorenbos, P. Ce^{3+} 5d-Centroid Shift and Vacuum Referred 4f-Electron Binding Energies of all Lanthanide Impurities in 150 Different Compounds. *J. Lumin.* **2013**, *135*, 93–104.
- (17) Ellens, A.; Meijerink, A.; Blasse, G. ^6I Emission and Vibronic Transitions of Eu^{2+} in KMgF_3 . *J. Lumin.* **1994**, *59*, 293–301.
- (18) Meijerink, A. Spectroscopy and Vibronic Transitions of Divalent Europium in LiBaF_3 . *J. Lumin.* **1993**, *55*, 125–138.
- (19) Blasse, G. Vibronic Transitions in Rare Earth Spectroscopy. *Int. Rev. Phys. Chem.* **1992**, *11*, 71–100.
- (20) Tanner, P. A.; Mak, C. S. K.; Edelstein, N. M.; Murdoch, K. M.; Liu, G.; Huang, J.; Seijo, L.; Barandiarán, Z. Absorption and Emission Spectra of Ce^{3+} in Elpasolite Lattices. *J. Am. Chem. Soc.* **2003**, *125*, 13225–13233.
- (21) Duan, C.-K.; Tanner, P. A.; Meijerink, A.; Makhov, V. 4f5d Transitions of Tb^{3+} in Cs_2NaYF_6 : The Effect of Distortion of the Excited-State Configuration. *J. Phys. Chem. A* **2011**, *115*, 9188–9191.
- (22) Ning, L.; Mak, C. S. K.; Tanner, P. A. High-Spin and Low-Spin f-d Transitions of Tb^{3+} in Elpasolite Hosts. *Phys. Rev. B: Condens. Matter Mater. Phys.* **2005**, *72*, 085127.
- (23) Kunkel, N.; Kohlmann, H.; Sayede, A.; Springborg, M. Alkaline-Earth Metal Hydrides as Novel Host Lattices for Eu^{II} Luminescence. *Inorg. Chem.* **2011**, *50*, 5873–5875.
- (24) Kunkel, N.; Meijerink, A.; Kohlmann, H. Bright Yellow and Green Eu(II) Luminescence and Vibronic Fine Structures in LiSrH_3 , LiBaH_3 , and Their Corresponding Deuterides. *Phys. Chem. Chem. Phys.* **2014**, *16*, 4807–4813.
- (25) Kunkel, N.; Meijerink, A.; Springborg, M.; Kohlmann, H. Eu(II) Luminescence in the Perovskite Host Lattices KMgH_3 , NaMgH_3 , and Mixed Crystals $\text{LiBa}_{1-x}\text{Sr}_x\text{H}_3$. *J. Mater. Chem. C* **2014**, *2*, 4799–4804.
- (26) Kunkel, N.; Böttcher, R.; Pilling, T.; Kohlmann, H.; Pöppel, A. Eu^{2+} -Containing Luminescent Perovskite-Type Hydrides Studied by Electron Paramagnetic Resonance. *Z. Phys. Chem.* **2016**, *230*, 931–942.
- (27) Kunkel, N.; Sontakke, A. D.; Kohaut, S.; Viana, B.; Dorenbos, P. Thermally Stimulated Luminescence and First-Principle Study of Defect Configurations in the Perovskite-Type Hydrides $\text{LiMH}_3\text{:Eu}^{2+}$ ($M = \text{Sr}, \text{Ba}$) and the Corresponding Deuterides. *J. Phys. Chem. C* **2016**, *120*, 29414–29422.
- (28) Marks, S.; Heck, J. G.; Habicht, M. H.; Oña-Burgos, P.; Feldmann, C.; Roesky, P. W. $[\text{Ln}(\text{BH}_4)_2(\text{THF})_2]$ ($\text{Ln} = \text{Eu}, \text{Yb}$) - A Highly Luminescent Material. Synthesis, Properties, reactivity, and NMR Studies. *J. Am. Chem. Soc.* **2012**, *134*, 16983–16986.
- (29) Schouwink, P.; Ley, M. B.; Tissot, A.; Hagemann, H.; Jensen, T. R.; Smrčok, L.; Černý, R. Structure and Properties of Complex Hydride Perovskite Materials. *Nat. Commun.* **2014**, *5*, 5706.
- (30) Kunkel, N.; Meijerink, A.; Kohlmann, H. Variation of the Eu^{II} Emission Wavelength by Substitution of Fluoride by Hydride in Fluorite-Type Compounds $\text{EuH}_x\text{F}_{2-x}$ ($0.20 \leq x \leq 0.67$). *Inorg. Chem.* **2014**, *53*, 4800–4802.
- (31) Kunkel, N.; Rudolph, D.; Meijerink, A.; Rommel, S.; Wehrich, R.; Kohlmann, H.; Schleid, T. Green Luminescence of Divalent Europium in the Hydride Chloride EuHCl . *Z. Anorg. Allg. Chem.* **2015**, *641*, 1220–1224.
- (32) Kunkel, N.; Kohlmann, H. Ionic Mixed Hydride Fluoride Compounds: Stabilities Predicted by DFT, Synthesis, and Luminescence of Divalent Europium. *J. Phys. Chem. C* **2016**, *120*, 10506–10511.
- (33) Rudolph, D.; Enseling, D.; Jüstel, T.; Schleid, T. Crystal Structure and Luminescence Properties of the First Hydride Oxide Chloride with Divalent Europium: $\text{LiEu}_2\text{HOCl}_2$. *Z. Anorg. Allg. Chem.* **2017**, *643*, 1525–1530.
- (34) Judd, B. R. Vibronic Contributions to Ligand-Induced Pseudo-Quadrupole Absorption of Rare Earth Ions. *Phys. Scr.* **1980**, *21*, 543–548.
- (35) McCumber, D. E.; Sturge, M. D. Linewidth and Temperature Shift of the R Lines in Ruby. *J. Appl. Phys.* **1963**, *34*, 1682–1684.
- (36) Equall, R. W.; Cone, R. L.; Macfarlane, R. M. Homogeneous Broadening and Hyperfine Structure of Optical Transitions in $\text{Pr}^{3+}\text{:Y}_2\text{SiO}_5$. *Phys. Rev. B: Condens. Matter Mater. Phys.* **1995**, *52*, 3963–3969.
- (37) Dorenbos, P. Thermal Quenching of Eu^{2+} 5d-4f Luminescence in Inorganic Compounds. *J. Phys.: Condens. Matter* **2005**, *17*, 8103–8111.
- (38) Ueda, J.; Dorenbos, P.; Bos, A. J. J.; Meijerink, A.; Tanabe, S. Insight Into the Thermal Quenching Mechanism for $\text{Y}_3\text{Al}_5\text{O}_{12}\text{:Ce}^{3+}$ Through Thermoluminescence Excitation Spectroscopy. *J. Phys. Chem. C* **2015**, *119*, 25003–25008.
- (39) Luminescence. *From Theory to Applications*; Ronda, C., Ed.; Wiley-CVH, 2008.
- (40) Greedan, J. E. Synthesis and Crystal Growth of SrLiH_3 and EuLiH_3 Ternary Hydrides with the Perovskite Structure. *J. Cryst. Growth* **1970**, *6*, 119–124.
- (41) Messer, C. E.; Eastman, J. C.; Mers, R. G.; Maeland, A. J. Ternary Perovskite Phases in Systems of Lithium Hydride with Barium, Strontium and Calcium Hydrides. *Inorg. Chem.* **1964**, *3*, 776–778.
- (42) Messer, C. E.; Levy, I. S. Systems of Lithium Hydride with Alkaline Earth and Rare Earth Hydrides. *Inorg. Chem.* **1965**, *4*, 543–548.
- (43) Kohlmann, H.; Yvon, K. The Crystal Structure of EuH_2 and EuLiH_3 by Neutron Powder Diffraction. *J. Alloys Compd.* **2000**, *299*, L16–L20.
- (44) Colognesi, D.; Celli, M.; Cilloco, F.; Newport, R. J.; Parker, S. F.; Rossi-Albertini, V.; Sacchetti, F.; Tomkinson, J.; Zoppi, M. TOSCA Neutron Spectrometer: The Final Configuration. *Appl. Phys. A: Mater. Sci. Process.* **2002**, *74*, S64–S66.
- (45) Parker, S. F.; Fernandez-Alonso, F.; Ramirez-Cuesta, A. J.; Tomkinson, J.; Rudic, S.; Pinna, R. S.; Gorini, G.; Castañón, J. F. Recent and Future Developments on TOSCA at ISIS. *J. Phys.: Conf. Ser.* **2014**, *554*, 012003.
- (46) Barrera, G. D.; Colognesi, D.; Mitchell, P. C. H.; Ramirez-Cuesta, A. J. LDA or GGA? A Combined Experimental Inelastic Neutron Scattering and Ab Initio Lattice Dynamics Study of Alkali Metal Hydrides. *Chem. Phys.* **2005**, *317*, 119–129.
- (47) Colognesi, D.; Barrera, G.; Ramirez-Cuesta, A. J.; Zoppi, M. Hydrogen Self-Dynamics in Orthorhombic Alkaline Earth Hydrides Through Incoherent Inelastic Neutron Scattering. *J. Alloys Compd.* **2007**, *427*, 18–24.
- (48) Kresse, G.; Furthmüller, J. Efficient Iterative Schemes for Ab Initio Total-Energy Calculations Using a Plane-Wave Basis Set. *Phys. Rev. B: Condens. Matter Mater. Phys.* **1996**, *54*, 11169–11186.
- (49) Kresse, G.; Furthmüller, J. Efficiency of Ab-Initio Total Energy Calculations For Metals and Semiconductors Using Plane-Wave Basis Sets. *Comput. Mater. Sci.* **1996**, *6*, 15–50.
- (50) Hafner, J. Ab initio Simulations of Materials Using VASP: Density-Functional Theory and Beyond. *J. Comput. Chem.* **2008**, *29*, 2044–2078.
- (51) Blöchl, P. E. Projector-Augmented Wave Method. *Phys. Rev. B: Condens. Matter Mater. Phys.* **1994**, *50*, 17953–17979.
- (52) Kresse, G.; Joubert, D. From Ultrasoft Pseudopotentials to the Projector Augmented-Wave Method. *Phys. Rev. B: Condens. Matter Mater. Phys.* **1999**, *59*, 1758–1775.
- (53) Perdew, J. P.; Burke, K.; Ernzerhof, M. Generalized Gradient Approximation Made Simple. *Phys. Rev. Lett.* **1996**, *77*, 3865–3868.
- (54) Togo, A.; Tanaka, I. First Principles Phonon Calculations in Materials Science. *Scr. Mater.* **2015**, *108*, 1–5.
- (55) Aroyo, M. I.; Perez-Mato, J. M.; Capillas, C.; Kroumova, E.; Ivantchev, S.; Madariaga, G.; Kirov, A.; Wondratschek, H. Bilbao Crystallographic Server I: Databases and Crystallographic Computing Programs. *Z. Kristallogr.* **2006**, *221*, 15–27.
- (56) Aroyo, M. I.; Kirov, A.; Capillas, C.; Perez-Mato, J. M.; Wondratschek, H. Bilbao Crystallographic Server II: Representations

of Crystallographic Point Groups and Space Groups. *Acta Crystallogr., Sect. A: Found. Crystallogr.* **2006**, *62*, 115–128.

(57) Hunt, G. R.; Perry, C. H.; Ferguson, J. Far-Infrared and Transmittance of Potassium Magnesium Fluoride and Magnesium Fluoride. *Phys. Rev.* **1964**, *134*, A688–A691.

(58) Maeland, A. J. Ternary Hydrides Possessing the Cubic Perovskite Structure. II. Vibration Spectra by the Inelastic Scattering of Cold Neutrons. *J. Chem. Phys.* **1969**, *51*, 2915–2919.

(59) Henderson, B.; Imbusch, G. *Optical Spectroscopy of Inorganic Solids*; Oxford Science Publications, 2010.

(60) Sears, V. F. Neutron Scattering Lengths and Cross Sections. *Neutron News* **1992**, *3*, 26–37.

(61) Maeland, A. J. Vibration Spectra of the Orthorhombic Alkaline-Earth Hydrides by the Inelastic Neutron Scattering of Cold Neutrons and Infrared Transmission Measurements. *J. Chem. Phys.* **1970**, *52*, 3952–3956.

(62) Ghebouli, B.; Ghebouli, M. A.; Fatmi, M. First-Principles Study of Structural, Elastic, Electronic and Optical Properties of Perovskite Hydrides XLiH_3 (X = Ba and Sr) Under Pressure. *Eur. Phys. J.: Appl. Phys.* **2010**, *51*, 20302.

(63) Yalcin, B. G.; Salmankurt, B.; Duman, S. Investigation of Structural, Mechanical, Electronic, Optical, and Dynamical Properties of Cubic BaLiF_3 , BaLiH_3 , and SrLiH_3 . *Mater. Res. Express* **2016**, *3*, 036301.

(64) Kittel, C. *Einführung in die Festkörperphysik*; Oldenbourg Wissenschaftsverlag, 2013.